PREDICTING SHRINKAGE STRESS FIELD IN CONCRETE SLAB ON ELASTIC SUBGRADE

By Wei Yang,[1] W. Jason Weiss,[2] and Surendra P. Shah[3]

ABSTRACT: Concrete is a material that changes volumetrically in response to moisture and temperature variations. Frequently, these volumetric changes are prevented by restraint from the surrounding structure, resulting in the development of tensile stresses. This paper provides a method for computing the stress and displacement fields that develop in response to this restraint by considering the concrete slab as a plate resting on an elastic foundation. The interface between the slab and the foundation is capable of simulating all cases between complete perfect bond and perfect compression/zero tension bond to permit debonding. In addition, stress relaxation is considered in the concrete to account for the reduction in stress due to creep/relaxation-related phenomena. For this reason, the stress-strain relationship and equilibrium equations have been considered in the rate or differential form. The history-dependent equilibrium equations are obtained by integrating the differential equations with respect to time. An example is presented to illustrate the favorable correlation that exists between the predicted behavior of the plate model and finite-element modeling.

INTRODUCTION

Concrete contracts in response to water loss or temperature reduction. The amount of shrinkage incurred depends on several factors including material composition, temperature, relative humidity, material maturity, and structural size. It should, however, be noted that free shrinkage alone is not sufficient to predict whether concrete will crack in service. Restraint from the surrounding structure prohibits the concrete from moving freely, and tensile stresses develop. The level of stress that develops is dependent on several factors, including degree of restraint, material stiffness, shrinkage rate, and amount of stress relaxation, whereas the potential for cracking is influenced by the stress level, specimen geometry, and the material's resistance to cracking. The development of tools capable of predicting cracking due to drying and thermal shrinkage in concrete structures is necessary, since cracks provide a path for corrosive agents to enter the concrete, thereby reducing the overall durability of the concrete structure. Recently, research in shrinkage cracking has attracted a great deal of interest, as illustrated in several theoretical and experimental studies (Bazant 1986; Springenschmid 1994; Blam and Bentur 1995; Yang et al. 1996; Bradford 1997; Shah et al. 1998; Weiss et al. 1998).

Recent research has focused on predicting the cracking behavior of thin laboratory specimens assuming uniaxial stress development for ring (Yang et al. 1996; Shah et al. 1998) and thin slab (Weiss et al. 1998) specimens. These models exhibited favorable correlation between the predicted age of cracking and experimentally observed trends for various concrete mixtures based on first principles that related the aging material properties with stress development and cracking behavior. This paper presents a modeling approach that is currently being developed to predict the stress development in thin-flat structures restrained by the foundation, in which early-age shrinkage cracking is often a problem. Examples of such structures include highway pavements, industrial floors, and bridge decks.

[1]Res. Asst. Prof., NSF Ctr. for ACBM, Dept. of Civ. Engrg., Northwestern Univ., 2145 Sheridan Rd., A130, Evanston, IL 60208-4400. E-mail: wya805@nwu.edu

[2]Res. Asst., NSF Ctr. for ACBM, Dept. of Civ. Engrg., Northwestern Univ., 2145 Sheridan Rd., A130, Evanston, IL. E-mail: jweiss@nwu.edu

[3]Walter P. Murphy Prof. of Civ. Engrg. and Dir., NSF Ctr. for ACBM, Northwestern Univ., 2145 Sheridan Rd., A130, Evanston, IL. E-mail: s-shah@nwu.edu

Note. Associate Editor: Arup Maji. Discussion open until June 1, 2000. To extend the closing date one month, a written request must be filed with the ASCE Manager of Journals. The manuscript for this paper was submitted for review and possible publication on January 29, 1999. This paper is part of the ***Journal of Engineering Mechanics***, Vol. 126, No. 1, January, 2000. © ASCE, ISSN 0733-9399/00/0001-0035–0042/$8.00 + $.50 per page. Paper No. 20038.

BACKGROUND

Due to the complexity of the aforementioned problem, researchers have solved shrinkage or temperature displacement and stress fields by introducing different simplifications. In the 1920s, Westergaard (1927) developed a thoretical treatment for dealing with a concrete slab resting on an elastic subgrade in which the reaction force was proportional to the deflected shape. Al-Nasra and Wang (1994) conducted a parametric study for concrete resting on an elastic foundation using a finite-element approach that permitted debonding and concrete softening; however, it did not include aging or stress relaxation. Mohamed and Hansen (1996) treated the pavement slab as a beam resting on an elastic foundation of a two-dimensional half plane using an ordinary differential equilibrium equation to describe the bending moment on an arbitrary cross section. Hong et al. (1997) established and solved the ordinary differential equation for the deflection of a beam resting on an in-plane Winkler's foundation (Nowacki 1962). In addition, many commercially available finite-element analysis packages can be used to compute stress and displacement fields of a viscoelastic material under thermal loading. These programs can be used to approximately compute shrinkage stress; however, since concrete exhibits aging viscoelastic behavior, the creep compliance is a function of both loading age and duration of loading. To simulate the behavior of concrete properly, the existing numerical packages must be modified.

MODELING APPROACH

The present research considers the concrete slab as an aging viscoelastic material resting on a semi-infinite elastic foundation, as shown in Fig. 1(a). Since the thickness of the slab is assumed to be small in comparison with the other two dimensions (thicknss/shortest width < 1/8), the slab can be considered as a plate. Eccentric restraint and nonlinear shrinkage gradients cause the slab to experience both bending and axial shortening. As a result, superposition has been used to combine pure bending and pure stretching as shown on an infinitesimal element in Fig. 1(b).

In general, the neutral plane of the plate experiences nonuniform bending deflection; as a result, the vertical component of stretching forces do not vanish and therefore contribute to the moment equilibrium equation of an infinitesimal element. Consequently, the products of the stretching forces and bend-

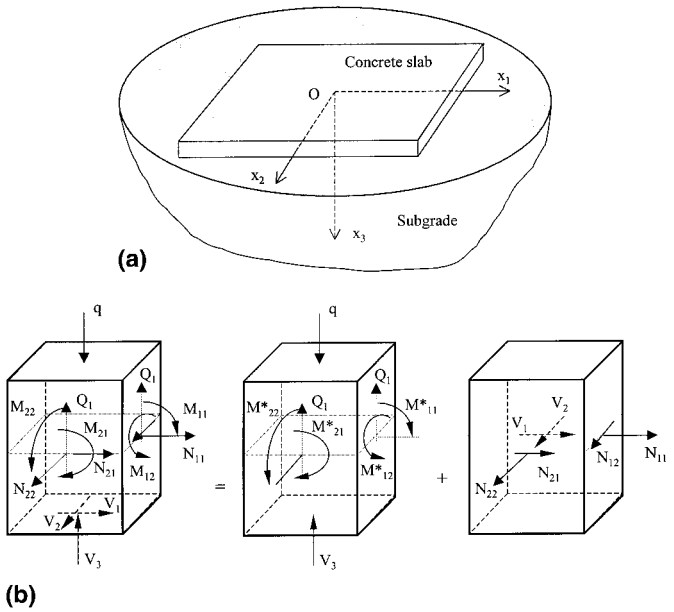

FIG. 1. (a) Concrete Slab Resting on Elastic Subgrade Considered as Semi-Infinite Half-Space; (b) Forces Applied on Arbitrary Differential Plate Element Can Be Separated as Superposition of Bending and Stretching Loads (* = Moments Caused by Frictional Tractions on Slab Bottom Surface Are Included)

ing curvatures appear in the differential equation and the problem becomes nonlinear. In the current solution, the writers neglect the nonlinear terms, since the deformations and curvatures are small.

The program computes the stress and displacement fields for a slab restrained from shrinkage based on first principles. Moisture and temperature strains were considered in a general manner. Stress relaxation was considered using a general aging compliance function of the form proposed by Müller (1994). The material properties needed for the programming include the elastic modulus (age-dependent) and Poisson's ratio of the concrete and subgrade. In addition, information is required to define the rate of free shrinkage strain as a function of depth and time.

FUNDAMENTAL EQUATIONS

As a result of stress relaxation, the shrinkage strain (ε_{ij}) is both age and history dependent. In previous research (Yang et al. 1996; Shah et al. 1998; Weiss et al. 1998), the incremental strain was considered to be composed of an instantaneous, time-dependent, and shrinkage strain-rate component. The incremental strain at any time t caused by a differential increment of stress σ_{ij} at time ξ ($0 \leq \xi \leq t$) can be expressed as

$$d\varepsilon_{ij}(t, \xi) = \frac{1}{E_\sigma(\xi)} \mathbf{C}_{ijkl}\, d\sigma_{kl}(\xi) + \frac{\varphi(t, \xi)}{E_c} \mathbf{C}_{ijkl}\, d\sigma_{kl}(\xi) + \delta_{ij}\alpha\, d\xi \quad (1)$$

In this equation, E_σ = elastic modulus at any time ξ; φ = creep function; E_c = reference elastic modulus (at 28 days); α = time rate of expansion/shrinkage; δ_{ij} = Kronecker delta; and the isotropic matrix $\mathbf{C}_{ijkl}$ is given by the following expression, in which ν is Poisson's ratio, which has been assumed to be constant with respect to time:

$$\mathbf{C}_{ijkl} = -\nu\delta_{ij}\delta_{kl} + (1 + \nu)(\delta_{ik}\delta_{jl} + \delta_{il}\delta_{jk}), \quad i, j, k, l = 1, 2, 3 \quad (2)$$

The creep function φ has been assumed to follow the form proposed by Müller (1994). The expansion rate for the free shrinkage (expansion) can be divided into two components, thermal and moisture shrinkage, as shown in the following:

$$\alpha(\xi) = \alpha_S + \alpha_T \dot{T} = \frac{d\varepsilon_{\text{moist}}(\xi)}{d\xi} + \alpha_T \frac{dT(\xi)}{d\xi} \quad (3)$$

where α_s = moisture-related shrinkage rate at time ξ; α_T = coefficient of thermal expansion; and $\dot{T}$ = derivative of temperature with respect to time. (Eq. (1) can be expressed in the rate form as

$$\dot{\varepsilon}_{ij} = \frac{1}{E_\sigma(\xi)} \mathbf{C}_{ijkl}\dot{\sigma}_{kl}(\xi) + \frac{\varphi(t, \xi)}{E_C} \mathbf{C}_{ijkl}\dot{\sigma}_{kl}(\xi) + \alpha(\xi)\delta_{ij} \quad (4)$$

where the strain and stress rates are given as $\dot{\varepsilon} = [\partial\varepsilon(t, \xi/\partial\xi]$ and $\dot{\sigma} = [d\sigma(\xi)/d\xi]$, respectively.

The stress rates must satisfy the sufficient and necessary conditions for equilibrium (assuming stress free initial condition). The equilibrium equations are

$$\dot{\sigma}_{ij,j} = 0, \quad (i, j = 1, 2, 3) \quad (5)$$

In addition, the following relationship is needed to ensure compatibility for the strain components:

$$\dot{\varepsilon}_{ij} = \frac{1}{2}(\dot{u}_{i,j} + \dot{u}_{j,i}), \quad (i, j = 1, 2, 3) \quad (6)$$

SUPERPOSITION OF BENDING AND STRETCHING

As previously mentioned, the deformation of a slab is generally caused by a combination of the bending and stretching components. Mansfield (1989) systematically described mechanical analysis of elastic plates under such loading conditions. In the following two subsections, the discussion is extended to bending and stretching of a concrete slab with aging viscoelastic material behavior.

Stretching Equations

As the slab shrinks, the in-plane stretching accounts for a large degree of the strain in the concrete slab. Fig. 2 describes both the resultant force on the side of the element acting on the neutral plane of the concrete slab (N) and the shear stress acting between the bottom surface of the slab (V) and the subgrade. The subscripts represent the corresponding direc-

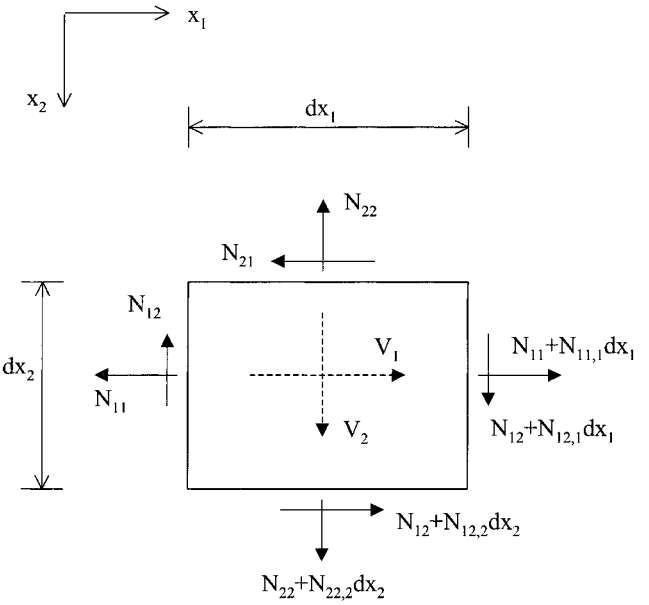

FIG. 2. Horizontal Force Components on Differential Plate (Slab) Element

tions. Applying equilibrium conditions to the Ox_1x_2 plane results in the following expression:

$$\dot{N}_{ij,j} + \dot{V}_i = 0 \tag{7}$$

If straining of the midplane of the plate due to deflection of the plate is ignored, the strains in the midplane are related to the forces per unit length as follows:

$$\dot{u}_{i,j} + \dot{u}_{j,i} = \frac{2}{\psi H}\,\mathbf{C}_{ijkl}\dot{N}_{kl} + \delta_{ij}\alpha \tag{8}$$

where H = depth of the slab; and ψ = stress relaxation function. To better consider aging behavior of concrete, the writers adopt the inversion of creep compliance that was proposed by Bazant and Kim (1979), which can be written as

$$\psi(t, \xi) = \frac{1 - \Delta_0}{J(t, \xi)} - \frac{0.115}{J(t, t - 1)}\left[\frac{J(\xi + \bar{t}, \xi)}{J(t, t - \xi)} - 1\right] \tag{9}$$

In this case, $J = (1/E_\sigma) + (\varphi/E_c)$; $\bar{t} = (1/2)(t - \xi)$; and Δ_0 is a variable coefficient.

By solving (8) for $\dot{N}_{kl}$, substituting the expression for $\dot{N}_{kl}$ into (7), and integrating the equations with respect to time, the fundamental stretching equations can be obtained:

$$\int_0^t \left[\frac{H}{1 - \nu^2}\,\dot{u}_{1,11} + \frac{H}{2(1 + \nu)}\,\dot{u}_{1,22} + \frac{H}{2(1 - \nu)}\,\dot{u}_{2,12}\right] \cdot \psi\, d\xi + V_1(t) = 0 \tag{10a}$$

$$\int_0^t \left[\frac{H}{1 - \nu^2}\,\dot{u}_{2,22} + \frac{H}{2(1 + \nu)}\,\dot{u}_{2,11} + \frac{H}{2(1 - \nu)}\,\dot{u}_{1,21}\right] \cdot \psi\, d\xi + V_2(t) = 0 \tag{10b}$$

In this expression, the time integral and spatial derivative are interchangeable and the initial condition of the pavement is assumed to be stress free.

Bending Equations

Let us now consider the state of stress in a plate with an arbitrary small deflection $u_3(x_1, x_2)$ [Fig. 3(a)]. A neutral plane is assumed to exist at the midheight of the slab; therefore, we shall focus attention on the state of strain, and hence the state of stress, in a plane at a distance x_3 from the mid-plane. The slopes of the midplane are $(\partial u_3/\partial x_1)$ and $(\partial u_3/\partial x_2)$, so the rates displacements $\dot{u}_1$ and $\dot{u}_2$ in the Ox_1x_2 plane at a distance x_3 from the midplane are given by

$$\dot{u}_i = -x_3\dot{u}_{3,i}, \quad (i = 1, 2) \tag{11}$$

The strain rates in this Ox_1x_2 plane are thus given by

$$\dot{\varepsilon}_{ij} = \frac{1}{2}\,(\dot{u}_{i,j} + \dot{u}_{j,i}) = -x_3\dot{u}_{3,ij}, \quad (i, j = 1, 2) \tag{12}$$

By inverting (4) and considering the geometrical relationships represented by (6) and (11), the following expression can be obtained for the bending stress rate:

$$\begin{Bmatrix}\dot{\sigma}_{11}\\ \dot{\sigma}_{22}\\ \dot{\sigma}_{12}\end{Bmatrix} = -\psi\begin{bmatrix}\frac{1}{1-\nu^2} & \frac{\nu}{1-\nu^2} & 0\\ \frac{\nu}{1-\nu^2} & \frac{1}{1-\nu^2} & 0\\ 0 & 0 & \frac{1}{2(1+\nu)}\end{bmatrix} \cdot \left\{x_3\begin{Bmatrix}\dot{u}_{3,11}\\ \dot{u}_{3,22}\\ \dot{u}_{3,12}\end{Bmatrix} - \alpha\begin{Bmatrix}1\\1\\0\end{Bmatrix}\right\} \tag{13}$$

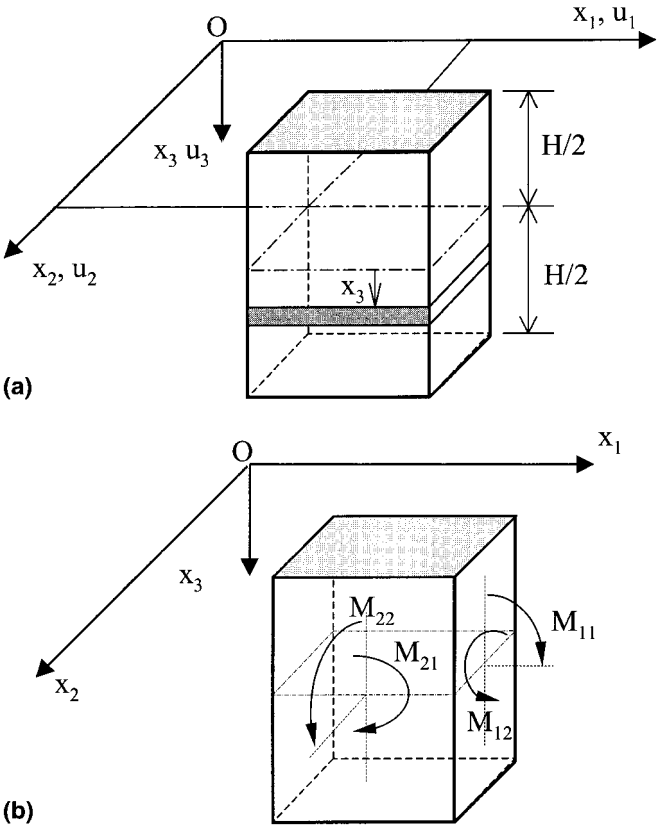

FIG. 3. Coordinates and Moments on Differential Plate (Slab) Element

These stress rate components vary linearly through the thickness of the plate and cause the moment rates per unit length acting on an element of the plate, as shown in Fig. 3(b). As a result, the following expressions can be obtained:

$$\dot{M}_{11} = \int_{-(1/2)H}^{(1/2)H} x_3\dot{\sigma}_{11}\, dx_3 = -D(\dot{u}_{3,11} + \nu\dot{u}_{3,22}) + \int_{-(1/2)H}^{(1/2)H}\frac{\psi}{1 - \nu}\,x_3\alpha\, dx_3 \tag{14a}$$

$$\dot{M}_{22} = \int_{-(1/2)H}^{(1/2)H} x_3\dot{\sigma}_{22}\, dx_3 = -D(\dot{u}_{3,22} + \nu\dot{u}_{3,11}) + \int_{-(1/2)H}^{(1/2)H}\frac{\psi}{1 - \nu}\,x_3\alpha\, dx_3 \tag{14b}$$

$$\dot{M}_{12} = \int_{-(1/2)H}^{(1/2)H} x_3\dot{\sigma}_{12}\, dx_3 = -D(1 - \nu)\dot{u}_{3,12} \tag{14c}$$

where the flexural rigidity of the plate, D, is defined by

$$D(t, \xi) = \frac{\psi(t, \xi)H^3}{12(1 - \nu^2)} \tag{15}$$

An equation of equilibrium may now be expressed in terms of derivatives of the moment rates and the applied loading (such as weight of concrete plate) as

$$\int_0^t \dot{M}_{ij,ij}\, d\xi - \frac{H}{2}\,V_{i,i}(t) + V_3(t) = q, \quad (i, j = 1, 2) \tag{16}$$

where q = weight of the concrete plate plus the superimposed load per unit area. If we denote

$$\kappa_s = \frac{12}{H^3}\int_{-(1/2)H}^{(1/2)H}\frac{\psi}{1 - \nu}\,x_3\alpha\, dx_3$$

and substitute (14) into (16), the expression for the general differential equation of a plate under shrinkage and creep can be obtained:

$$\int_0^t [\nabla^2(D\nabla^2\dot{u}_3) - (1-\nu)\diamond^4(D, \dot{u}_3) + (1+\nu)\nabla^2(D\kappa_s)]\, d\xi$$

$$-\frac{H}{2} V_{i,i}(t) + V_3(t) = q \tag{17}$$

in which

$$\nabla^2 = \partial^2/\partial x_1^2 + \partial^2/\partial x_2^2,\ \diamond^4(D, \dot{u}_3) \equiv D_{,11}\dot{u}_{3,22} - 2D_{,12}\dot{u}_{3,12} + D_{,22}\dot{u}_{3,11}$$

It should be noted that the spatial differentiation and time integration in (17) are exchangeable. If the pavement is considered to be homogeneous with uniform thickness and uniform shrinkage in horizontal plane (i.e., the free shrinkage rate is only a function of depth), the bending equation can be rewritten simply as

$$\int_0^t D\nabla^4\dot{u}_3\, d\xi - \frac{H}{2} V_{i,i}(t) + V_3(t) = q, \quad (i = 1, 2) \tag{18}$$

These are the differential integral equations the writers used to represent bending effects. For large deformation problems, the products of curvatures and stretching forces are not to be neglected and the nonlinear term $\int_0^t N_{ij}\dot{u}_{3,ij}\, d\xi$ will be added to the right-hand side of (18) or (17).

SUPPORT FROM ELASTIC FOUNDATION

Some research has been conducted by simplifying the pavement as an elastic or viscoelastic beam resting on an elastic foundation with a restoring pressure that is proportional to the deflection [Winkler's foundation; see, e.g., Nowacki (1962); Hong et al. (1997)]. Using this approach, the resultant pressure acting on the plate has the form $q_{res} = q - k\dot{w}$, where k = foundation modulus (or spring constant). The differential equation for the deflection of the plate can then be obtained using preceding analysis by substituting q_{res} for q.

In this paper, the foundation below the pavement has been assumed to be a three-dimensional, elastic half space. The bond between pavement and foundation has been incorporated to include two conditions—either perfect bond or perfect bond when the normal force is in compression and zero bond occurs whenever there is tension. In addition, the formulation provided in this paper is also valid for various degrees of interfacial tensile bond; however, it has not been used in the calculations provided below.

The interaction forces can be computed using a Green's function approach, as described in the following paragraph. Consider an arbitrary point X at the top surface of the foundation. The displacements caused by forces transmitted from the pavement to the foundation can be written as follows:

$$u_i(X) = \int\int_{A'} U_{ij}^*(X, Y)V_j(Y)\, dS(Y) \tag{19}$$

where Y = point where the force components $V_j\, dS$ are applied; A' = bond area between the pavement and foundation; and $U_{ij}^*(X, Y)$ = Green's function, which represents the displacement in the Ox_i direction at point X caused by a unit point load in the Ox_j direction at point Y. Green's functions of this type can be found in theory of elasticity books (e.g., Xu 1992); however, for the reader's convenience, these functions are included in Appendix I.

BOUNDARY CONDITIONS

Most commonly, the slab sides are traction free. By denoting the normal and tangential directions at the free edge using the subscripts n and τ, respectively, the boundary conditions for bending equations can be written as

$$M_{nn} = 0 \text{ (no bending moment at free edge)} \tag{20a}$$

$$M_{n\tau} = 0 \text{ (no twisting moment)} \tag{20b}$$

$$Q_n = 0 \text{ (no shearing force)} \tag{20c}$$

$$R = 0 \text{ (no concentrated reaction force at corner points)} \tag{20d}$$

The second and the third equations listed above can be simplified to one condition that is derived from considering the resultant of the shear force flow on the cross section of an infinitesimal plate element. Representing the conditions mentioned above in terms of displacements, the boundary conditions can be correspondingly written as

$$\int_0^t D(\dot{u}_{3,nn} + \nu\dot{u}_{3,\tau\tau})\, d\xi + \int_0^t \int_{-(1/2)H}^{(1/2)H} x_3\psi\alpha(x_3, \xi)\, dx_3\, d\xi = 0 \tag{21a}$$

$$\int_0^t D[\dot{u}_{3,nnn} + (2-\nu)\dot{u}_{3,n\tau\tau}]\, d\xi = 0 \tag{21b}$$

$$\int_0^t D\dot{u}_{3,n\tau}\, d\xi = 0 \tag{21c}$$

In addition to satisfying the boundary conditions at the edges of pavement, the stretch free conditions are also to be satisfied:

$$N_{nn} = 0,\ N_{n\tau} = 0 \tag{22a,b}$$

Eq. (22a) represents a zero normal stretching force at the neutral plane, while (22b) signifies that no tangential force exists. The equivalent forms of these equations represented by displacement components are

$$\int_0^t \frac{\psi}{1+\nu}(\nu\dot{u}_{n,n} + \dot{u}_{\tau,\tau})\, d\xi - \int_0^t \int_{-(1/2)H}^{(1/2)H} \psi\alpha(x_3, \xi)\, dx_3\, d\xi = 0 \tag{23a}$$

$$\int_0^t \psi(\dot{u}_{n,\tau} + \dot{u}_{\tau,n})\, d\xi = 0 \tag{23b}$$

These boundary conditions are represented in the differential form with respect to spatial coordinates, and these are lower-order derivatives comparable to the differential equations presented earlier.

NUMERICAL STRATEGY

Two stretching differential equations (10), one bending (18), and three boundary integral equations (19) were combined to solve for the six direct unknown functions of space and time. These functions describe the three displacement components (u_i) and the three traction-interaction components (V_i). The displacement and stress fields were solved numerically by converting the differential and boundary integral equations into a group of coupled finite-difference and boundary element equations. The complete set of equations used to solve this problem includes fundamental stretching and bending differential integral equations (10) and (18), the inplane stretching boundary conditions [(23)], the plate free-edge bending conditions [(21)], and the foundation boundary integral equations [(19)].

Problem Discretization

In the work presented here, time differentiation in all equations was discretized using a backward-difference method. Spatial derivatives were discretized using a central-differencing approach for both differential equations and boundary conditions. The stretching differential equations are second order [(8)]. Therefore, a fictitious layer of nodes was added beyond the plate boundary by discretizing the differential equations into finite-difference equations. The additional unknowns gen-

erated by those fictitious nodes were automatically made solvable by introducing the normal and shear traction boundary conditions [(23)].

Since the differential equations established from bending equilibrium conditions [(18)] are fourth order, two fictitious layers of nodes were introduced by converting the bending-differential equations into linear algebraic equations using central differencing. Additional unknowns were compensated for by introducing free boundary conditions for bending, twisting, and shear at the regular boundary points and free boundary conditions for bending, twisting, shear, and concentrated reactions at the corner points [(21)].

The surface of the foundation covered by the plate was discretized into a mesh projected by the finite-difference mesh used for the stretching and bending equations. Numerical integration on each four-node isoparametric element was performed by Gauss integration with 10×10 interpolation points.

Debonding is judged by monitoring whether the tensile traction at the slab-subgrade interface reaches a critical level. Once the tensile traction at a node point is found in excess of the given critical value, the numerical computation starts a loop to release the restraint at that node point, then the released tractions in all three directions are redistributed to the neighboring nodes. Numerical integration moves on to the next time step on condition that the tensile tractions at all nodes are below the critical value.

Convergence

At the current stage, since the writers focused on simulation of the stress and displacement fields of pavements at early ages, time differentiation and integration are discretized in equal ranges. It was confirmed numerically that, for realistic values of the rate of shrinkage strain and the age-dependent elastic modulus, for the first 10 days, displacements and stresses tend to be stable or converge within 30 steps. That is, an eight-hour increment was found to be sufficient for the first 10 days. After the initial 10 days, the rate of change of shrinkage strain, elastic modulus, and creep compliance reduces. As a result, a larger time step can be adopted. Optimizing the application of this numerical method for long-time calculations would require variational time increments.

Convergence of this approach in the spatial dimension follows the general rules of the finite-difference method in 2-dimensional and the boundary-element method in 3-dimensional senses. Since in many cases, deformation and bottom interface stress of a pavement do not change severely, elements having twice the plate depth can provide solutions of sufficient accuracy.

NUMERICAL EXAMPLES

Simple Thermal Stress Solution Compared with FEA Results

The numerical approach presented in this paper was compared with a commercially available finite-element solution (CSA/NASTRAN), by considering a thermal stress analysis. Creep and aging effects were neglected and the plate was considered to rest on an elastic subgrade. The plate was assumed to have a 12×12 m^2 footprint and a 0.2 m thickness. The plate was considered to have the properties of a normal strength concrete with $E = 30$ GPa, $\nu = 0.2$, and $\alpha_T = 2.0 \times 10^{-6}$/°C. The foundation was assumed to have the properties of dense sand with $E = 50$ MPa and $\nu = 0.35$. No instantaneous temperature stresses were applied to the foundtion (i.e., $\alpha_{T\_foundation} = 0$). An instantaneous temperature drop ($\Delta T = -50$°C) was applied to the entire slab, which resulted in the development of deformations and stresses. It should be noted that the bond between the plate and the foundation was assumed to be perfect (i.e., no debonding).

The finite-element analysis computation was conducted by discretizing a quarter of the plate and the foundation into a finite-element mesh due to the symmetry of the problem. The plate was meshed by quadrilateral plate elements with an 8×8 grid. The elastic foundation was discretized using three-dimensional, eight-node, quadrilateral elements with an identical size for the elements adjacent to the plate. The size of the foundation elements was increased gradually as the distance from the plate surface increased. To approximately simulate the natural boundary condition at infinity, the foundation is fixed at a distance of ten times the half-length of the plate.

In the computational analysis, using the code developed from the present work, schemes of up to 24×24 elements (25×25 nodes) were adopted for the horizontal plane. The computations trials in this analysis have shown that a mesh finer than 12×12 elements (13×13 nodes) resulted in a variation of stresses less than five percent that from the finest mesh. The comparison of displacement on a line in the midplane and stress at the top surface in the Ox_1 direction obtained from both the proposed method and the finite-element model (FEM) are shown in Figs. 4(a and b), respectively.

It is seen that the horizontal displacements obtained from different programs coincided perfectly. On the inner points, stresses also match reasonably. It should be noted that in the present approach, boundary stresses are determined by boundary conditions, yet in FEM, stresses are inter- or extrapolated from node displacement solutions. This is why large stress differences are observed at slab edges.

Linear Shrinkage Gradient through Depth

To simulate a typical pavement slab, the displacement and stress fields were calculated using an 8×8 m^2 footprint with a 0.33 m thickness. The plate was of normal strength concrete

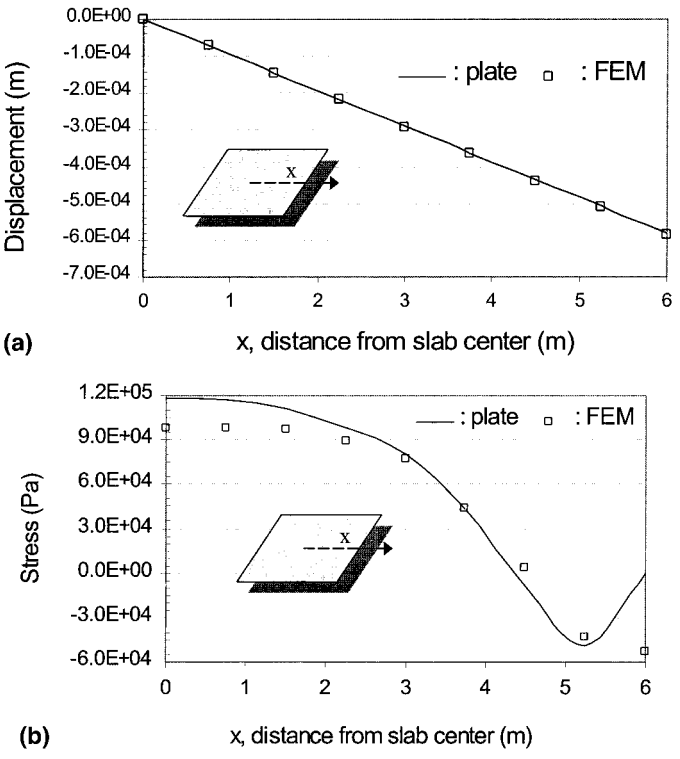

FIG. 4. (a) Comparison of Horizontal Displacements on Neutral Plane Obtained from Developed Code with FEM; (b) Comparison of Normal Stresses, σ_{11}, on Top of Slab Obtained from Developed Code with FEM

with E_{28} = 30 GPa and ν = 0.2 at all times. As described by Müller (1994), the elastic modulus changes over time following $E_\sigma(\xi) = E_{28} \cdot \exp[0.5s(1 - (28/(\xi/t_1))^{0.5})]$ with s = 0.25 and t_1 = 1 day. To compute the creep compliance, the compressive strength and relative humidity of the ambient environment, as required by the CEB model (Müller 1994), were specified as 30 MPa and 40%, respectively. The free shrinkage rate of the slab was assumed to be linear through the depth with no free shrinkage at the plate foundation interface and a shrinkage rate at the top surface of the form $\dot{\varepsilon}_{shrink} = 10^{-4} - 5 \times 10^{-5} \ln(t)$ when $t \in [1, 10]$ (days). The mathematical expression for the shrinkage rate was obtained using regression analysis of free shrinkage data (Yang et al. 1996; Shah et al. 1998; Weiss et al. 1998). The foundation was again considered to be dense sand E = 50 MPa and Poisson's ratio ν = 0.35. It should be noted that the shrinkage profile can be any function in depth and in time and the solution presented here is only a simple example problem to provide a description of the behavior of a slab under shrinkage. Debonding was considered using a perfect compression–zero tension bond law.

Fig. 5 shows the displacement of the neutral plane in the horizontal direction (Ox_1) and the displacement in the vertical direction (Ox_3) after 10 days. The results indicate that the horizontal displacement is typically less at the center than at the edges due to debonding. Vertical deflections are higher near the free edges, especially at the corners of the slab; however, the middle of the slab is virtually flat.

The area of the slab that debonded can be determined by using the interaction-traction plots shown in Fig. 6. The tractions are zero in the debonded region; however, these tractions are high between the bonded and debonded regions of the plate and nearly minimal in the case of the frictional tractions, and the vertical reaction component is similar to the slab weight in the center of the plate. The increase in tractions at the area near the debonding region is caused by the interaction force redistribution after the bond between the slab and the foundation is released.

The stress components of the slab at the top surface are shown in Fig. 7. All normal stress components in the Ox_1-Ox_2 directions are in tension. As expected, normal and principal stresses are highest in the center portion of the slab. It can be seen that, in the center portion of the slab, the results are relatively constant. Using a systematic solution process for the slab, the maximum tensile stress development over time can be predicted. In addition, by maintaining the slab depth and materal properties constant, the other dimensions of the slab can be varied appropriately to provide variation of the maximum tensile stress versus the slab dimension. Coupling this analysis technique with the age-dependent tensile strength of the concrete material provides an estimation for the crack or joint spacing in a concrete pavement; however, future work will be aimed at incorporating a fracture mechanics failure criterion with this approach.

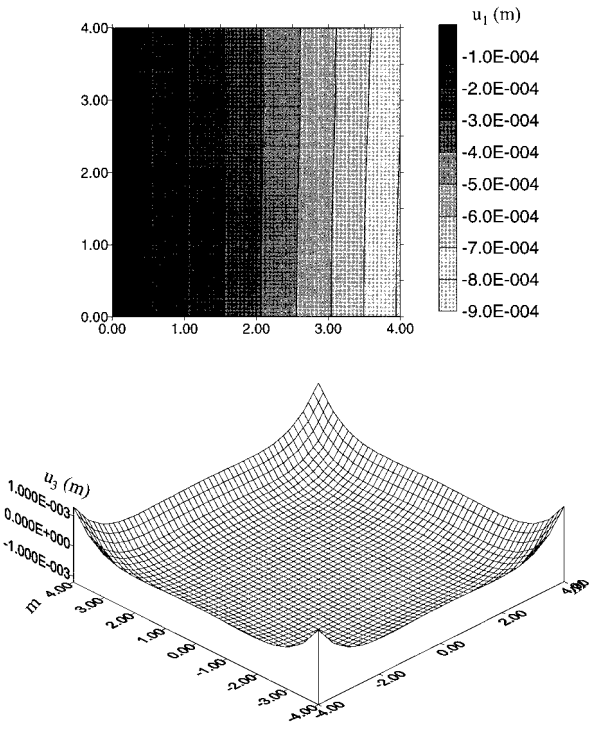

FIG. 5. Displacement Contour Plot of u_1 in Quarter of Slab (Top) and Deflected Surface (u_3) of Whole Slab (Bottom)

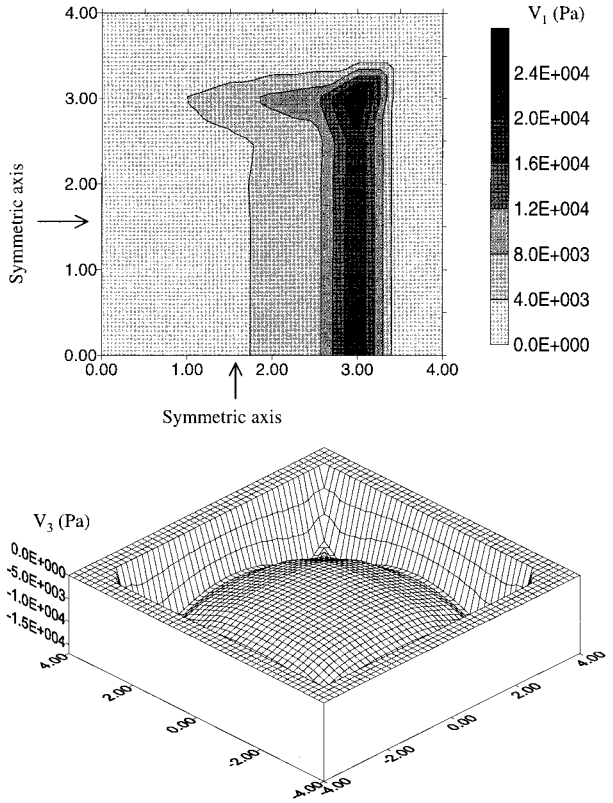

FIG. 6. Contour Plot of Interface Frictional Traction V_1 (Top) in Ox_1 Direction of Quarter of Slab and Normal Supporting Component V_3 for Whole Slab

SUMMARY AND CONCLUSIONS

In this work, a technique was developed to compute the stress development in a three-dimensional concrete plate restrained by an elastic subgrade. The following list provides a synopsis of the advantages of this program:

1. Stress relaxation with aging: Time-dependent behavior results in the inability to integrate the time integration of the functions appearing in differential equations in a closed form. For this reason, the solution of differential equations was carried out incrementally with respect to time. During the numerical computation, displacement and traction solutions of all the previous steps need to be saved to obtain the solution of a new time step. The present approach only requires meshing in a two-dimensional plane; thus computation time is drastically reduced.
2. Elastic subgrade: For the purpose of simulating stresses in pavements, the foundation is treated as an elastic half-space. Based on the calculations conducted in this re-

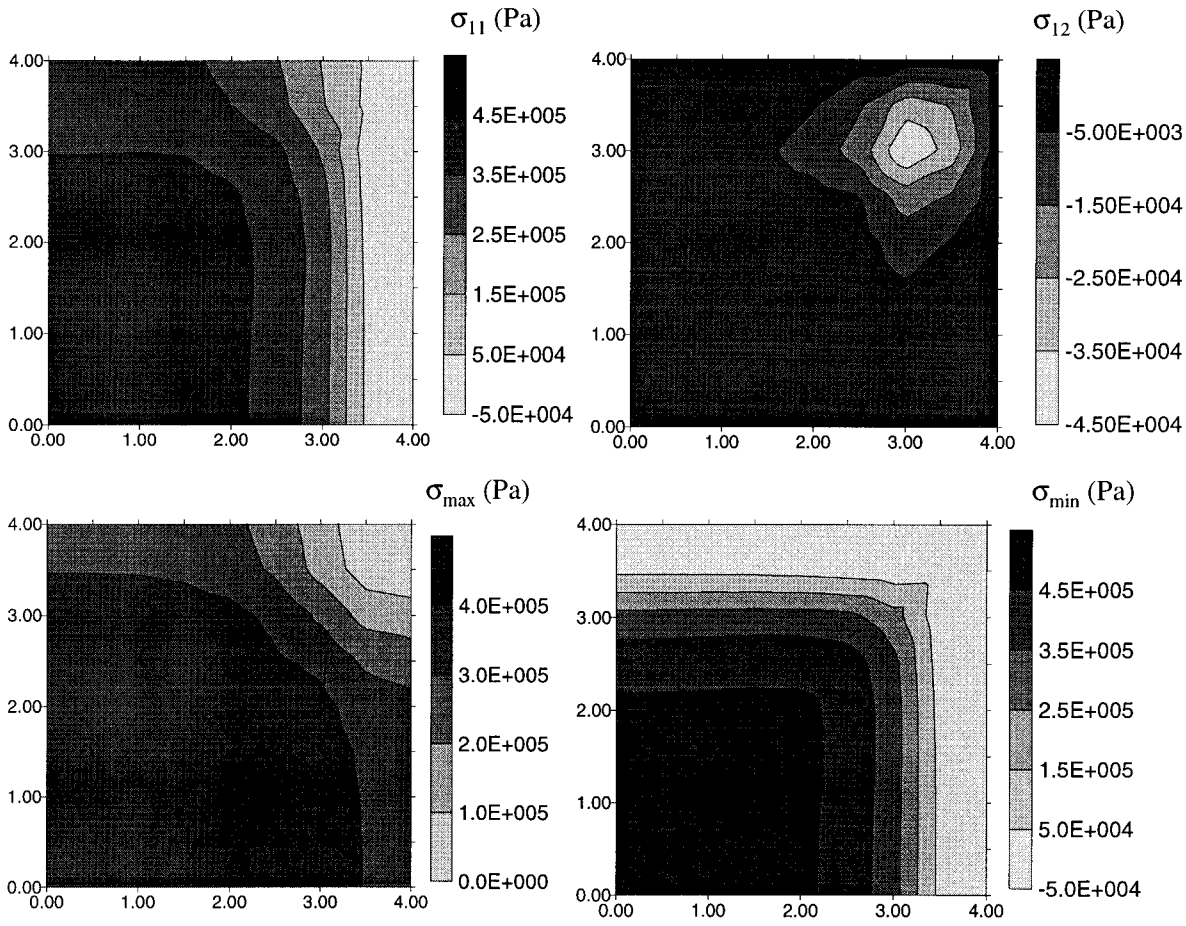

FIG. 7. Contour Plots of Normal (σ_{11}, Top Left) and Shear (σ_{12}, Top Right) Stresses for Top Surface of Quarter of Slab; Contour Plots of Maximum (Bottom Left) and Minimum (Bottom Right) Principal Stresses

search, frictional restraint forces provided by the subgrade are significant and can not be ignored. Therefore, in addition to the vertical stiffness of the elastic support, consideration of stiffness in the horizontal direction is also important. The discretized boundary integral equations are linear algebraic equations in which only the traction components in the pavement-subgrade interface are involved. Even so, the coefficient matrix is a full matrix, and its dimension is fairly small compared with other methods that require further discretization.

3. Debonding: In reality, the bonding strength of the slab-subgrade interface can vary dramatically. For instance, in a concrete-soil interface it can be close to zero, whereas in a concrete-concrete interface it is on the level of material tensile strength. In many cases associated with the debonding phenomenon, frictional sliding occurs at the bottom of a slab, so the Columb-Mohr criterion is more suitable for application. To simplify the numerical analysis at the present stage, avoiding the iteration process for nonlinear calculation, a friction-independent tensile strength criterion is adopted. During numerical analysis, debonding is tested for every single time step; i.e., stress redistribution is completed at each step where debonding occurred.

Analysis of the displacement and stress fields in a three-dimensional concrete slab considering shrinkage and creep is a complex task, requiring a thorough understanding of the time-dependent material behavior. Using the approach presented in this paper, the stress and displacement fields can be predicted for a concrete slab restrained by an elastic subgrade during shrinkage. By properly adjusting slab boundary conditions and the elastic properties of the foundation, this model can also be extended to simulate stress and displacement fields of other flat concrete structures, such as floors or bridge decks.

APPENDIX I. GREEN'S FUNCTIONS IN (19)

The Green functions in (19) can be written as [$X = (x_1, x_2)$, $Y = (\bar{x}_1, \bar{x}_2)$]:

$$U_{ii}^{*} = \frac{1 + \nu}{\pi E r}\left[1 - \nu + \nu\frac{(x_i - \bar{x}_i)^2}{r^2}\right],$$

no sum on $i(= 1, 2)$, $\quad r = \sqrt{(x_1 - \bar{x}_1)^2 + (x_2 - \bar{x}_2)^2}$

$$U_{12}^{*} = U_{21}^{*} = \frac{\nu(1 + \nu)}{\pi E r^3}(x_1 - \bar{x}_1)(x_2 - \bar{x}_2)$$

$$U_{3i}^{*} = -\frac{(1 + \nu)(1 - 2\nu)}{2\pi E r^2}(x_i - \bar{x}_i), \quad i = 1, 2$$

$$U_{33}^{*} = \frac{1 - \nu^2}{\pi E r}, \quad U_{i3}^{*} = -U_{3i}^{*}, \quad i = 1, 2$$

where E and ν = elastic modulus and Poisson's ratio, respectively.

If, for example, ox_1 and ox_2 are both symmetric axes, with the following substitutions:

$$U_{i1}^{*} = U_{i1}^{*}(x_1, x_2, \bar{x}_1, \bar{x}_2) + U_{i1}^{*}(x_1, x_2, \bar{x}_1, -\bar{x}_2)$$
$$- U_{i1}^{*}(x_1, x_2, -\bar{x}_1, \bar{x}_2) - U_{i1}^{*}(x_1, x_2, -\bar{x}_1, -\bar{x}_2)$$
$$U_{i2}^{*} = U_{i2}^{*}(x_2, x_2, \bar{x}_1, \bar{x}_2) + U_{i2}^{*}(x_1, x_2, \bar{x}_1, -\bar{x}_2)$$
$$+ U_{i2}^{*}(x_1, x_2, -\bar{x}_1, \bar{x}_2) - U_{i2}^{*}(x_1, x_2, -\bar{x}_1, -\bar{x}_2)$$

$$U_{i3}^{*} = U_{i3}^{*}(x_2, x_2, \bar{x}_1, \bar{x}_2) + U_{i3}^{*}(x_1, x_2, \bar{x}_1, -\bar{x}_2)$$

$$+ U_{i3}^{*}(x_1, x_2, -\bar{x}_1, \bar{x}_2) + U_{i3}^{*}(x_1, x_2, -\bar{x}_1, -\bar{x}_2)$$

integration is over the first quarter of the plate footprint.

ACKNOWLEDGMENTS

This research was carried out at the National Science Foundation Center for Science and Technology for Advanced Cement-Based Materials (ACBM), headquartered at Northwestern University. The funding received from Grace Construction Products, a Division of W. R. Grace Co., Connecticut, during the course of this study has been greatly appreciated.

APPENDIX II. REFERENCES

Al-Nasra, M., and Wang, R. L. (1994). ''Parametric study of slab-on-grade problems due to initial warping and point loads.'' *ACI Struct. J.*, 91(1), 198–210.

Bazant, Z. P., and Kim, S.-S. (1979). ''Approximate relaxation function for concrete.'' *J. Struct. Div.*, ASCE, 105(12), 2695–2705.

Banzant, Z. P., ed. (1986). *Creep and Shrinkage of Concrete: Mathematical Modeling; Proc., 4th RILEM Int. Symp.*, RILEM, Cachan Cedex, France.

Bloom, R. A., and Bentur, A. (1995). ''Free and restrained shrinkage of normal and high-strength concretes.'' *ACI Mat. J.*, 92(2), 211–217.

Bradford, M. A. (1997). ''Shrinkage behavior of steel-concrete composite beams.'' *ACI Struct. J.*, 94(6), 625–632.

Hong, A. P., Li, Y. N., and Bazant, Z. P. (1997). ''Theory of crack spacing in concrete pavements.'' *J. Engrg. Mech.*, ASCE, 123(3), 267–275.

Mansfield, E. H. (1989). *Bending and stretching of plates*. Cambridge University Press, Cambridge, U.K.

Mohamed, A. R., and Hansen, W. (1996). ''Prediction of stresses in concrete pavements subjected to non-linear gradients.'' *Cement and Concrete Compos.*, 18, 381–387.

Müller, H. S. (1994). *New prediction models for creep and shrinkage of concrete*. American Concrete Institute, Detroit, Mich.

Nowacki, W. (1962). *Thermoelasticity*. Pergamon Press, Tarrytown, N.Y.

Shah, S. P., Ouyang, C., Marinkunte, S., Yang, W., and Becq-Giradoun, E. (1998). ''A method to predict shrinkage cracking of concrete.'' *ACI Mat. J.* July–August, 339–346.

Springenschmid, R., ed. (1994). *Thermal Cracking in Concrete at Early Ages; Proc., Int. RILEM Symp.*, RILEM, Cachan Cedex, France.

Weestergaard, H. M. (1927). ''Analysis of stresses in concrete roads caused by variations of temperature.'' *Public Roads*, 8(3), 54–60.

Weiss, W. J., Yang, W., and Shah, S. P. (1998). ''Shrinkage cracking of restrained concrete slabs.'' *J. Engrg. Mech.*, ASCE, 24(7), 765–774.

Yang, W., Wang, K., and Shah, S. P. (1996). ''Predictions of concrete cracking under coupled shrinkage and creep conditions. *Mat. for the New Millennium; Proc., 4th Mat. Engrg., Conf.*, ASCE, New York, 564–573.

Xu, Z. (1992). *Applied elasticity*. Wiley, New York.